Soret-Driven Convection Inside Concentric Porous Spheres Saturated by Binary Fluid

Khairi Sioud, Ali Abdennadher, Slim Kaddeche, Marie Catherine Charrier Mojtabi, Abdelkader Mojtabi

Soret driven convection inside concentric porous spheres saturated by binary fluid: Comparison with parallelepipedic vertical column

Khairi Sioud[1,2†], Ali Abdennadher[2†], Slim Kaddeche[3†], Marie Catherine Charrier-Mojtabi[1†] and Abdelkader Mojtabi[1*†]

[1*]Institut de Mécanique des Fluides de Toulouse (IMFT), Université de Toulouse, CNRS, France.
[2]Université de Carthage, EPT, LIM (LR 01-ES-13), 2078, La Marsa, Tunisie.
[3]Université de Carthage, INSAT, MMA (LR 11-ES-25), 1080, Tunisie.

*Corresponding author(s). E-mail(s): mojtabi@ imft.fr;
†These authors contributed equally to this work.

Abstract

The columns commonly used for the species separation of a binary fluid, are very thin vertical parallelepipedic columns, filled with a porous medium (i.e. TGC columns). This species separation is due to the mass flux induces by the thermal gradient applied on walls of the cavity namely the Soret effect, in the gravity field. In this paper a new configuration used to study the species separation in a binary fluid was presented. The evolution of species separation in a binary fluid saturating a porous media, in a cavity between two concentric spheres, was studied analytically and numerically. The thickness of the cavity is $\boldsymbol{e = R_o - R_i}$, where $\boldsymbol{R_i}$ and $\boldsymbol{R_o}$ are the internal and external radii respectively. First, an analytical solution was developed using the parallel flow approximation considering $\boldsymbol{e \ll R_i}$. The analytical results obtained are in a good agreement with the numerical ones performed with a spectral method or Comsol Multiphysics software. Thus, the results in the spherical configuration were compared with those obtained in a porous TGC column of same thickness, $\boldsymbol{e}$, height, $\boldsymbol{H = \pi R_i}$ and depth,

$\boldsymbol{L = 2R_o}$.The numerical and analytical studies showed that the differences in mass fractions, $\boldsymbol{C_{max} - C_{min}}$, and the time needed to obtain the stationary separation starting from a homogeneous binary solution were almost equal in the two configurations.The amount of species separated is greater in the spherical configuration than in the vertical column used.

Keywords: Heat and Mass Transfer, Porous Media, Species separation, Soret effect, Thermogravitational columns, Spherical cell, Binary mixture, Numerical simulations

1 Introduction

Species separation in binary or multicomponents mixture is a coupled heat and mass transfer phenomena.

Pure thermo-diffusion leads to very weak species separation in binary mixtures. To increase the species separation in the presence of a gravity field, many authors use thermo-gravitational diffusion in vertical, fluid or porous, columns (TGC) ([1]-[5]). These TGC are parallelepipedic cavities consisting of two vertical plates facing each other. The plates are maintained at uniform temperatures, $T_h > T_c$. The spacing between these two parallel plates is millimetric. The other faces of the cavity are perfectly insulated. The combination between the convective flow, generated by the horizontal thermal gradient and the thermodiffusion between the two plates, leads to a stationary convective state and a constant vertical mass gradient. Often, one of the components of the binary mixture has particular industrial importance for pharmacy or perfumery, or has high added value components (rare earths). The Soret effect in liquid mixtures has been completely reviewed by Köhler et al. [6].

In 1959, Lorenz and Emery [2] considered columns (TGC) filled with porous packing saturated by a binary fluid to allow the use of columns with spacing higher than one millimetre.

Until the 2000s, research on thermo-gravitational diffusion concerned mainly vertical columns. In 2003, Platten et al. [7] performed an experimental study of the effect of the tilt with respect to the horizontal direction, of a rectangular cell heated only from below.

Since 2007, various works aimed at improving species separation using different configurations and processes. Charrier-Mojtabi et al. [8] showed that it was possible to obtain the species separation in a horizontal cell heated from below by studying the influence of the separation ratio and the normalized porosity on the stability of the equilibrium solution, theoretically and numerically. Elhajjar et al. [9] stablished that it was possible to achieve separation in the horizontal configuration when the separation factor was negative or greater than a positive value leading to the onset of a unicellular flow. They demonstrated that the maximum separation remained unchanged when the TGC was tilted from its vertical position to the horizontal position [10]. Khouzam et al.

[11] used mixed convection in order to study the species separation in a binary mixture in a horizontal cell. Yacine et al. [12] studied the case of a porous cavity saturated by a binary mixture that was subjected to cross heat fluxes. V.Yasnou et al. [13] studied experimentally the transient mass transfer associated with a thermal gradient through a liquid mixture containing a layer of porous medium saturated with liquid. Mojtabi et al. [14] studied the influence of the thermophysical characteristics of the walls in the process for separating the constituents of a binary mixture. They showed that separation was underestimated when the effect of the thermal characteristics of the walls was not taken into account. Recently, Mojtabi et al. [15] considered a new configuration to separate the binary components mixture in a horizontal porous layer by moving the walls of the cavity. On the over hand, thermogravitational separation and time to reach the steady state were studied recently by Seta et al. [16].

In the present study, species separation in a porous cavity between two concentric spheres and a TGC column, saturated with a water-ethanol mixture, was compared. The separation corresponds to the difference in mass fractions between the two ends of the TGC and between the top and the bottom parts of the spherical cavity. The species separation and the time to reach the steady state leading to maximum separation were evaluated in both configurations.

An analytical solution was obtained in the case of a TGC. The velocity field and the mass fraction gradient along the z-vertical axis were then calculated. The analytical results were corroborated by direct 2D and 3D numerical simulations.

For the spherical configuration, an analytical solution of the axisymmetric laminar unicellular flow was obtained for the first time to our knowledge. 2D and 3D numerical studies were carried out using Comsol Multipysics software and a spectral code, in order to validate the analytical results. The results obtained with these different methods are in good agreement. The times to reach the stationary state and the separation in both configurations were compared.

2 Mathematical formulation

The two porous cavities studied are respectively the porous cavity saturated by a binary mixture between two concentric spheres and the vertical parallelepipedic column (TGC). These cavities have the same thickness, $e = R_o - R_i$, where R_i and R_o are the internal and external radii of the spherical cavity respectively. $H = \pi R_i$ is the height and the depth, $L = 2R_o$ of the TGC. This height corresponds to the length of the convective cell, which develops within the spherical cavity even for the lowest values of the temperature difference $(T_h - T_c)$. The two porous cavities are saturated with water (60.88 wt %)-ethanol mixture. The cavities considered in this study are shown schematically in Fig. 1.

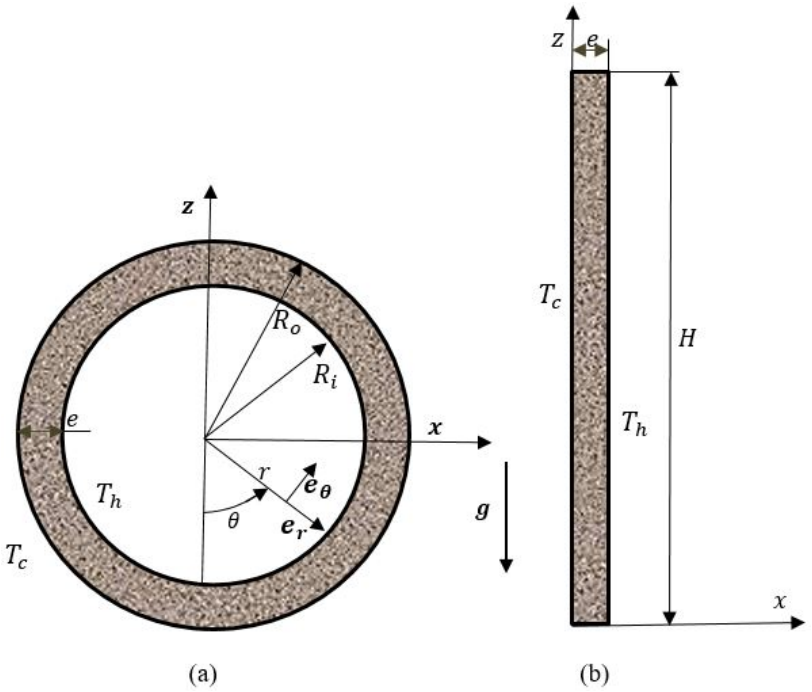

Fig. 1 Schematic diagram of the concentric spheres (a) and the TGC column (b)

The Boussinesq approximation is assumed to be valid; thus, the thermophysical properties of the binary fluid are constant, except for the density in the buoyancy term, which varies linearly with the local temperature, T, and the local mass fraction, C, of the denser component:

$$\rho = \rho_0(1 - \beta_T(T - T_{ref}) - \beta_C(C - C_{ref})) \tag{1}$$

where β_T and β_C are respectively the thermal and mass expansion coefficients of the binary fluid, defined as follows: $\beta_T = \frac{-1}{\rho_0}(\frac{\partial \rho}{\partial_T})_C > 0$, $\beta_C = \frac{-1}{\rho_0}(\frac{\partial \rho}{\partial_C})_T < 0$. In a binary fluid mixture subjected to a temperature gradient, a mass fraction gradient appears due to the thermodiffusion or Soret effect. In addition to the usual expression for the mass flux density $\mathbf{J}_m$ given by Fick's law, a part due to the temperature gradient (namely the Soret effect) was used so that:

$$\mathbf{J}_m = -\rho D^* \boldsymbol{\nabla} C - \rho {D'_T}^* \boldsymbol{\nabla} T \tag{2}$$

where D^* and ${D'_T}^*$ are respectively the mass diffusion coefficient and the thermodiffusion coefficient of the denser component in porous media, ρ is the mixture density, T the temperature and C the mass fraction of the constituent of interest ${D'_T}^*$ is often written as: ${D'_T}^* = F(C)D^*_T$ where $F(C)$ is a particular function satisfying $F(C = 0) = 0$ and $F(C = 1) = 0$. In many studies, the authors consider that $F(C) = C(1 - C) \simeq C_0(1 - C_0)$, where $C_0 = C_{ref}$ is

initial mass fraction. The previous assumptions lead to a new form of equation (2):

$$\mathbf{J}_m = -\rho(D^*\boldsymbol{\nabla}C - C_0(1-C_0){D_T}^*\boldsymbol{\nabla}T) \tag{3}$$

The dimensional mathematical formulation of the physical problem is given by:

$$\begin{gathered}\boldsymbol{\nabla}\cdot\boldsymbol{V} = 0\\ \boldsymbol{V} = -\frac{K}{\mu}(\boldsymbol{\nabla}P - \rho_0[1-\beta_T(T-T_0)-\beta_C(C-C_0)]\boldsymbol{g})\\ (\rho c)^*\frac{\partial T}{\partial t} + (\rho c)_f\boldsymbol{V}\cdot\boldsymbol{\nabla}T = \lambda^*\boldsymbol{\nabla}^2T\\ \epsilon^*\frac{\partial C}{\partial t} + \boldsymbol{V}\cdot\boldsymbol{\nabla}C = D^*\boldsymbol{\nabla}^2C + {D_T}^*C_0(1-C_0)\boldsymbol{\nabla}^2T\end{gathered} \tag{4}$$

In these equations, $(\rho c)^*$ and λ^* are respectively the effective heat capacity and the thermal conductivity of the porous medium, ϵ^* its porosity and K its permeability. μ and ρ_0 are the dynamic viscosity and the density, at $T = T_0$ of the saturating fluid. The corresponding boundary conditions for the TGC and concentric spheres are respectively:
(5) for the TGC:

$$\begin{gathered}x = 0, x = e;\ \boldsymbol{V}\cdot\boldsymbol{x} = 0, T(0,y,z) = T_h, T(e,y,z) = T_c, \mathbf{J}_m\cdot\boldsymbol{x} = 0\\ y = 0, y = L;\ \boldsymbol{V}\cdot\boldsymbol{y} = 0, \frac{\partial T}{\partial y} = \frac{\partial C}{\partial y} = 0\\ z = 0, z = \pi R_i;\ \boldsymbol{V}\cdot\boldsymbol{z} = 0, \frac{\partial T}{\partial z} = \frac{\partial C}{\partial z} = 0\end{gathered} \tag{5}$$

and (6) for the concentric spheres ($\boldsymbol{e_r}, \boldsymbol{e_\theta}, \boldsymbol{e_\phi}$):

$$\begin{gathered}r = R_i;\ T = T_h, \boldsymbol{V}\cdot\boldsymbol{n} = 0, \mathbf{J}_m\cdot\boldsymbol{n} = 0\\ r = R_o;\ T = T_c, \boldsymbol{V}\cdot\boldsymbol{n} = 0, \mathbf{J}_m\cdot\boldsymbol{n} = 0\\ \theta = 0, \pi, \forall\phi, \frac{\partial T}{\partial\theta} = \frac{\partial C}{\partial\theta} = 0, \boldsymbol{V}\cdot\boldsymbol{e_\theta} = 0\end{gathered} \tag{6}$$

where $\mathbf{n}$ denotes the unit normal vector to the surfaces of the spheres. The flow between the two concentric spheres is assumed to be axisymmetric.

3 Analytical resolution

3.1 For TGC column

To solve the system of equations (4) associated with the boundary conditions (5) analytically in the case of TGC, for $e \ll \pi R_i$, the forgotten effect hypothesis [7] and parallel flow approximation [17] are used. The parallel flow

approximation leads to unicellular flow given by:

$$\mathbf{V}_u = W_u(x)\boldsymbol{z}, T_u = f(x), C_u = mz + h(x) \tag{7}$$

where m is an unknown constant that represents the mass fraction gradient in the $\mathbf{z}$ direction. With these assumptions and for the steady state, the system of equations (4) with the boundary conditions (5) is reduced to the following set of equations, which can be solved using Maple software:

$$\begin{gathered} \frac{\partial W_u}{\partial x} = \frac{K}{\mu}\rho_0\beta_T\frac{\partial T}{\partial x} \\ \boldsymbol{\nabla}^2 T = 0 \\ m\ W_u - D^*\boldsymbol{\nabla}^2 C_u - D_T^* C_0(1-C_0)\boldsymbol{\nabla}^2 T_u = 0 \end{gathered} \tag{8}$$

Using the boundary conditions (5), we deduce the expression for the temperature, the velocity and the mass fraction field, given by the following expressions:

$$\begin{gathered} T_u = \frac{(T_c - T_h)}{e}x + T_h \\ W_u = \frac{Kg\beta_T(T_c - T_h)(2x - e)}{2e\nu} \\ C_u = mz + \frac{(T_c - T_h)}{D^*}\left(\frac{mKg\beta_T(e^3 - 6ex^2 + 4x^3)}{24e\nu} - D_T^* C_0(1-C_0)\left(\frac{x}{e} - \frac{1}{2}\right)\right) \end{gathered} \tag{9}$$

The value of the mass fraction gradient m:

$$m = \frac{-10Kg\nu\beta_T D_T^* C_0(1-C_0)(T_c - T_h)^2}{(Keg\beta_T(T_c - T_h))^2 + 120(\nu D^*)^2} \tag{10}$$

is obtained by specifying that the total mass flux of the component of mass fraction C, through any cross section of the TGC parallel to the $\mathbf{x}$ axis, is equal to zero:

$$\int_0^e \left(W_u C_u - \left(D^*\frac{\partial C_u}{\partial z} + D_T^* C_0(1-C_0)\frac{\partial T_u}{\partial z}\right)\right)dx = 0 \tag{11}$$

Application to the separation of a water-ethanol binary mixture: To illustrate the analytical results obtained in this study, we restrict ourselves to the experimental values of the thermophysical parameters of a water (60.88 wt%)-ethanol (39.12 wt%) solution studied Platten et al. [7]. The values of the thermophysical properties of this binary solution, at the average temperature $T_0 = 22.5°C$ are given in Table 1.

Costesèque et al. [18] showed that the Soret coefficients in free and porous

Table 1 Properties for a water (60.88 wt%) - ethanol (39.12 wt%) mixture at a mean temperature of 22.5°C

$D[\mathrm{m^2 s^{-1}}]$	$D_T[\mathrm{m^2 (s\ K)^{-1}}]$	β_C	$\beta_T[\mathrm{K^{-1}}]$	$\alpha[\mathrm{m^2 s^{-1}}]$	$\rho_0[\mathrm{kg\ m^{-3}}]$	$\nu[\mathrm{m^2 s^{-1}}]$
$4.32\ 10^{-10}$	$1.37\ 10^{-12}$	-0.212	$7.86\ 10^{-4}$	10^{-7}	935.17	$2.716\ 10^{-6}$

media can be considered as equal. On the other hand, the values of the mass diffusion coefficients and of the thermal diffusion coefficients are different for these two media. The mass and thermal diffusion coefficients of the component of interest are deduced from the coefficients D and DT in a fluid medium by means of the following relations $D^* = D/2.30$ and ${D_T}^* = D_T/2.30$.

3.2 For the spherical configuration

Here, the assumptions used to determine the analytical solution in a TGC column are extended to the resolution of system of equations (4) associated with boundary conditions (6) in the case of concentric spheres with $e \ll R_i$. The parallel flow approximation leads to the unicellular flow given by:

$$\boldsymbol{V_u} = V_r(r,\theta)\boldsymbol{e_r} + V_\theta(r,\theta)\boldsymbol{e_\theta}, \tag{12}$$

With these assumptions and for the steady state, the system of equations (4) with boundary conditions (6) is reduced to the following set of equations (13), which is solved using Maple software:

$$\begin{gathered}
\boldsymbol{\nabla}\cdot\boldsymbol{V_u} = 0 \\
\boldsymbol{V_u} = \frac{K}{\mu}(-\nabla P + \rho_0 g[1-\beta_T(T_u - T_0)](\cos(\theta)\boldsymbol{e_r} - \sin(\theta)\boldsymbol{e_\theta})) \\
\boldsymbol{\nabla}^2 T_u = 0 \\
V_r(r,\theta)\frac{\partial C_u}{\partial r} + V_\theta(r,\theta)\frac{\partial C_u}{r\partial\theta} = D^*\boldsymbol{\nabla}^2 C_u {D_T}^* C_0(1-C_0)\boldsymbol{\nabla}^2 T_u
\end{gathered} \tag{13}$$

Using the stream function, ψ, with $V_r = \partial\psi/(\partial\theta\ r^2\sin\theta)$ and $V_\theta = -\partial\psi/(\partial r\ r\sin\theta)$, the continuity equation is automatically checked.

$$\frac{\partial^2\psi}{\partial r^2} + \frac{1}{r}\frac{\partial^2\psi}{\partial\theta^2} + \frac{\cos(\theta)}{r^2\sin\theta}\frac{\partial\psi}{\partial\theta} = -\frac{K}{\mu}\rho_0 g\beta_T\frac{\partial T_u}{\partial r}r\sin^2(\theta) \tag{14}$$

By setting $\psi = \varphi(r)\sin^2(\theta)$, in equation (14), we deduce the equation verified by the function φ:

$$\frac{\partial^2\varphi}{\partial r^2} - 2\frac{\varphi}{r^2} = -\frac{K}{\mu}\rho_0 g\beta_T\frac{\partial T_u}{\partial r} \tag{15}$$

Using boundary conditions (6), we deduce the expression for the temperature and the velocity given by the following expressions:

$$T_u = \frac{1}{R_o - R_i}(R_i R_o (T_h - T_c)/r + R_o T_c - R_i T_h)$$
$$V_r = \frac{2\cos(\theta)}{r^2}\varphi(r)$$
$$V_\theta = -\frac{\sin(\theta)}{r}\frac{\partial \varphi(r)}{\partial r} \tag{16}$$

where:

$$\varphi(r) = \frac{\frac{K}{\mu}\rho_0 g \beta_T (T_h - T_c)(R_o - r)(R_i - r)((R_o + r)R_i + rR_o)R_i R_o}{2r(R_o - R_i)(R_o^2 + R_i R_o + R_i^2)} \tag{17}$$

It can thus be deduced that the velocity intensity is proportional to: $\frac{K}{\mu}\rho_0 g \beta_T (T_h - T_c)$. Knowing the temperature and velocity fields, given by equation (16), we deduce the mass fraction equation:

$$\frac{\partial^2 C_u}{\partial r^2} + \frac{1}{r^2}\frac{\partial^2 C_u}{\partial \theta^2} + \frac{2}{r}\frac{\partial C_u}{\partial r}(1 - \frac{\cos(\theta)}{r}\frac{\varphi(r)}{D^*}) - \frac{2}{r^2}\frac{\partial C_u}{\partial \theta}(\frac{\cos(\theta)}{\sin(\theta)} - \frac{\sin(\theta)}{D^*}\frac{\partial \varphi(r)}{\partial r}) = 0 \tag{18}$$

4 Numerical results

The dimensionless set of equations (4) with boundary conditions (5) for (TGC) and (6) for concentric spheres, were solved numerically using a finite element code (Comsol Multiphysics) and a spectral collocation method [19] on Gauss-Lobatto-Chebyshev points. A time-dependent solver and the set of equations (incompressible Darcy equation, energy and mass diffusion equations) in transient form were used. The condition of conservation of the average mass fraction in the two different porous cavities saturated by a binary fluid was imposed on each iteration. For the spherical configuration, the spectral collocation method on Gauss-Lobatto-Chebyshev points in the radial direction was combined with the Fourier spectral method for the polar angle. Indeed the interpolated functions are periodic with respect to the polar angle due to the spherical geometry and the boundary conditions considered. Direct numerical simulations were performed for cavities of the same thickness, $e = 6.10^{-3}$ m, $(e = R_o - R_i)$, with $R_i = 0.05, 0.1, 0.2, 0.3$ m. The height of the TGC was equal to $H = \pi R_i$. This height was chosen so that the length of the stream function lines was almost equal in the two considered configurations. The physical mechanism inside the two configurations was the same, as well as the structure of the flow. Thus, the species separation would be expected to be of the same order of magnitude in the vertical column and the spherical cell. This result that was subsequently confirmed numerically. For numerical applications, constant temperatures, $T_h = 25°\text{C}$ and $T_c = 15°\text{C}$,were imposed on the walls of

the two configurations and for two values of the permeability, $K = 2.5\ 10^{-11}\mathrm{m}^2$ and $K = 5.66\ 10^{-11}\mathrm{m}^2$. The initial mass fraction $C_0 = C_{ref} = 0.6088$ was also kept constant in both configurations.

4.1 Comparison between analytical results and numerical simulations for TGC

In the vertical thermogravitational column, the thermal fields obtained analytically and numerically were almost identical. Fig.2 (a) presents the values of the velocity, W_u, as a function of x for $z = H/2$, since the velocity is an independent function of z, except in the neighbourhood of $z = 0$ and H. The plot of the mass fraction C_u versus z for $x = e/2$ in Fig. 2 (b) shows very good agreement between the analytical and numerical results.

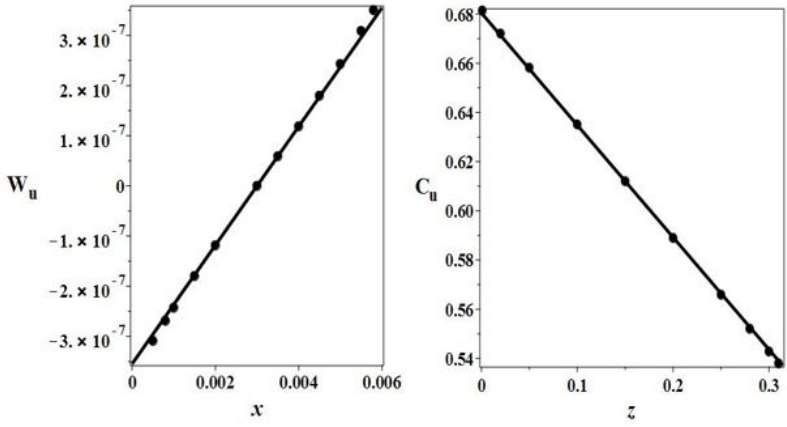

Fig. 2 (a) (on left) velocity, $W_u(x, z = H/2)$ and (b) (on right) mass fraction $C_u(x = e/2, z)$, obtained analytically (continuous line) and using direct numerical simulation (dotted line)

The maximal and minimal values of mass fraction, C_{max} and C_{min}, respectively, for four TGC of the same thickness, $e = 6.10^{-3}$m, obtained using analytical and direct numerical simulations are given in Table 2. The results presented show very good agreement between the numerical results and the analytical ones.

4.2 Comparison between analytical results and numerical simulations for a porous cavity between two concentric spheres

In concentric spheres, the values of thermal field according to r, $T_u(r, \theta = \pi/2)$, obtained analytically and numerically are in very good agreement (cf. Fig. 4).

Table 2 Maximal and minimal mass fraction in TGC for $e = 6.10^{-3}$m, for different values of $H(Ri = 0.05;\ 0.1;\ 0.2;\ 0.3$ m), obtained analytically and by direct numerical methods

Mass Fraction of TGC		Analytical results	Spectral method	Comsol
H=0.157 m	C_{max}	0.646	0.646	0.646
	C_{min}	0.572	0.572	0.572
H=0.314 m	C_{max}	0.681	0.680	0.680
	C_{min}	0.537	0.537	0.537
H=0.628 m	C_{max}	0.752	0.750	0.750
	C_{min}	0.466	0.468	0.468
H=0.942 m	C_{max}	0.822	0.819	0.819
	C_{min}	0.395	0.398	0.398

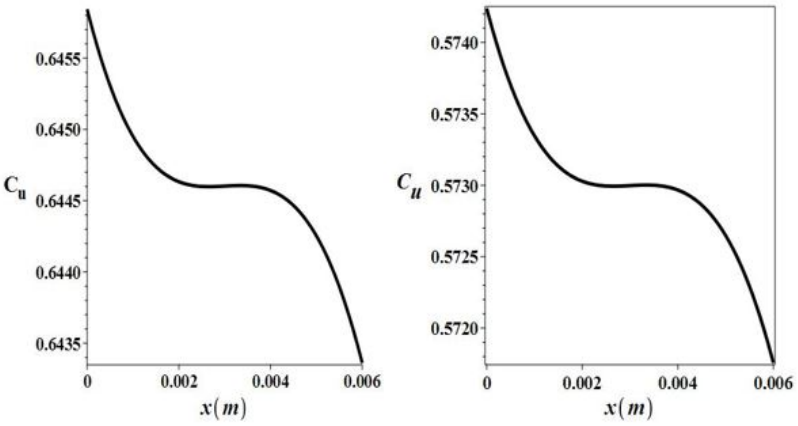

Fig. 3 (a) (on left) mass fraction $C_u(x, z = 0)$, and (b) (on right) mass fraction $C_u(x, z = \pi R_i = 0.157)$, obtained analytically

The plot of the tangential velocity, $V_\theta(r, \theta = \pi/2)$, versus r in Fig. 5 (a) and the plot of the radial velocity $V_r(r, \theta = 3\pi/4)$, in Fig. 5 (b) also show very good agreement between the analytical and the numerical results.

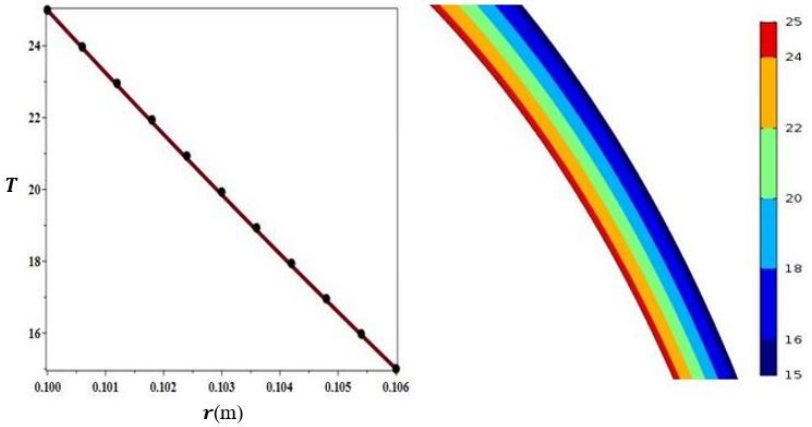

Fig. 4 (a) (on left) temperature $T(r, \theta = \pi/2)$, obtained analytically (continuous line) and using direct numerical simulation (dotted line), (b) (on right), isothermal lines for $0.05 \leq z \leq 0.08$ m

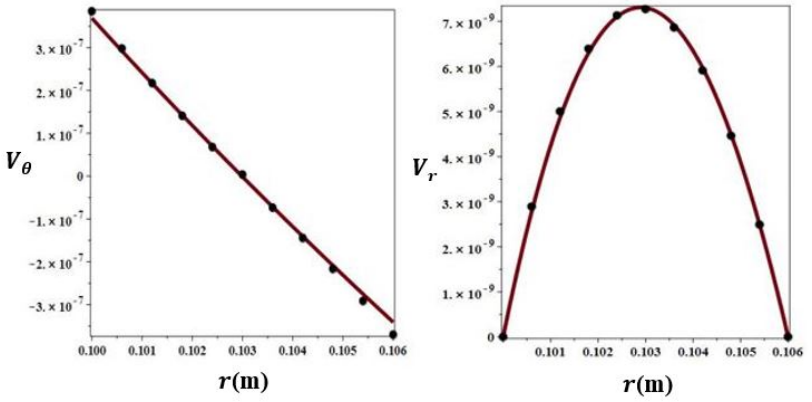

Fig. 5 (a) (on left) tangential velocity $V_\theta(r, \theta = \pi/2)$, (b) (on right), radial velocity $V_r(r, \theta = 3\pi/4)$, obtained analytically (continuous line) and using direct numerical simulations (dotted line)

Below we present the streamlines in the upper part of the spherical configuration Fig. 6 (b). The comparison between the values of the stream function $\psi(r, \theta = \pi/2)$, obtained analytically and numerically are in good agreement (Fig. 6 (a)).

The values of maximal, C_{max}, and minimal, C_{min}, mass fraction for 4 spherical configurations, with the same thickness, $e = 6.10^{-3}$m, obtained using two direct numerical simulation approaches, are given in Table 3. The result presented shows a very good agreement between the two numerical approaches used in the present work. The values obtained for C_{max} and C_{min}, in Table 2 for the vertical column and in Table 3 for the spherical cavity,

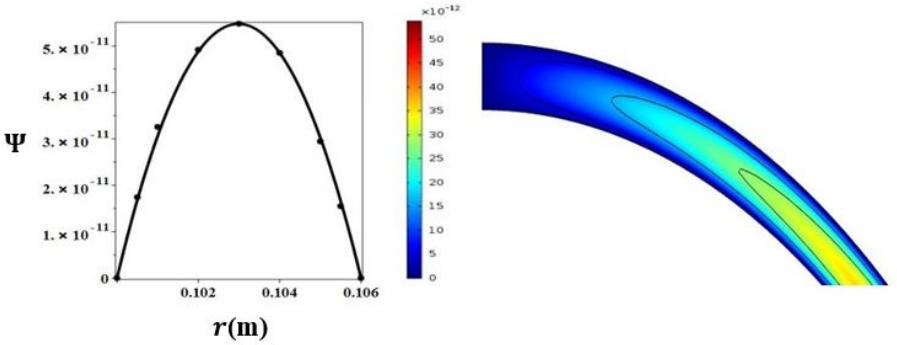

Fig. 6 (a) (on left) stream function $\psi(r, \theta = \pi/2)$, obtained analytically (continuous line) and numerically (dotted line), (b) (on right), streamlines obtained numerically for $\frac{5\pi}{6} \leq \theta \leq \pi$ and for every azimuthal plane $\phi = \phi_0$ considered

Table 3 Comparison of the maximal and minimal mass fractions, C_{max} and C_{min}, respectively, in concentric spheres for $e = R_o - R_i = 6.10^{-3}$m and for different values of Ri, obtained using the spectral collocation method and Comsol software

Mass Fraction		Spectral method	Comsol Multiphysics
$R_i = 0.05$ m	C_{max}	0.651	0.651
	C_{min}	0.565	0.565
$R_i = 0.1$ m	C_{max}	0.687	0.687
	C_{min}	0.527	0.527
$R_i = 0.2$ m	C_{max}	0.759	0.760
	C_{min}	0.452	0.452
$R_i = 0.3$ m	C_{max}	0.832	0.833
	C_{min}	0.376	0.377

showed that the maximum separation obtained $(C_{max} - C_{min})$ for each of the four values of the radii Ri studied is slightly greater in the spherical cell. For the spherical cells corresponding to $Ri = 0.05, 0.1, 0.2, 0.3$m, $(C_{max} - C_{min}) = 0.086, 0.160, 0.308, 0.456$ while for TGC: $(C_{max} - C_{min}) = 0.074, 0.143, 0.282, 0.421$. The respective ratios of the species separation in these two configurations $(1.16, 1.12, 1.09, 1.08)$ show that the species separation in the spherical cavity is of the order of 1.1 times greater than the separation obtained in the vertical column.

4.3 Flow stability in the upper part of spherical configuration or around its symmetrical part

The direct numerical simulations obtained (§4.2), in the case where the porous medium is saturated by a binary fluid with a positive Soret coefficient showed that the flows obtained are stable. The instability in this configuration may

happen either in the upper part or around the its symmetrical part. Indeed, as the inner sphere is maintained at $T_h > T_c$, the temperature of the outer sphere, and the difference of the radii of the two spheres verifies $R_0 - R_i = e = 6 \times 10^{-3}$ m $\ll R_i$ then locally the top and the bottom of the spherical configuration can be assimilated respectively to porous plane layers saturated by a binary fluid. The top layer is heated from below and the bottom one is heated from above. In the upper part, the heaviest constituent migrates towards the upper wall, which is colder, leading to a loss of flow stability for a Rayleigh number higher than $Ra_c = \frac{12}{Le\varphi}$, where Le is the Lewis number of the binary fluid in the porous layer and φ , the separation factor, Cf. [8]. For a water-ethanol binary mixture saturating the porous medium, the Lewis number is $Le = 654,86$ and $\varphi = 0.406$ which gives $Ra_c = 0.045$. For this experimental configuration, the Rayleigh number, $Ra = \frac{g\beta(T_h - T_c)}{\alpha\nu} Ke$, is equal to 0.0143 since Ra is proportional to the product of the thickness, $e = 6 \times 10^{-3}$ m, by the permeability of the medium which is of the order of 10^{-10}.
To conclude with, for our configuration $Ra < Ra_c$ and the flow is stable. For the bottom layer, it is locally a plane layer heated from above, the heaviest constituent which migrates towards the bottom wall leads to an infinitely stable layer.
For a negative Soret coefficient, the heaviest constituent migrates upwards from the hot inner sphere. Locally, the plane layer is heated from below and the binary fluid being denser at the bottom of that layer, the critical Rayleigh number is then greater than $4\pi^2$, see [8]. In the symmetrical part, there is locally a plane layer heated from above, but the binary fluid is denser along the hot wall, a situation that could become unstable.

5 Time to reach the stationary state in the TGC and in the spherical configuration

The numerical simulations, using the spectral collocation method and the Comsol Multipysics software, allow us to calculate the time necessary to reach the stationary state. The calculations were performed for two values of $R_i = 0.1, 0.2$ m and $H = \pi R_i$.
In Table 4 for the TGC and Table 5 for spherical cell, the values of C_{max} and C_{min} corresponding to four physical times during the evolution of C towards the stationary state are presented.
It emerges from Table 4 that the values of C_{max} and C_{min} calculated from the Comsol software and from the spectral code are very close with a maximal discrepancy of 10^{-4}.
The mass fractions C_{max} and C_{min}, as a function of time in the vertical column and the spherical configuration, are presented, in Fig. 7 and Fig. 8 respectively. It emerges from the analysis of these two figures that the species separation is slightly higher in the spherical configuration ($C_{max} = 0.623$) than for the TCC column ($C_{max} = 0.613$)
In addition, in the spherical cavity, the stationary state in the lower part is

Table 4 Variation of C_{max} and C_{min}, in TGC, from the initial uniform state C_0, to the stationary non uniform state for $H = 0.314$ m, $H = 0.628$ m, and $e = 6.10^{-3}$m obtained using the spectral method and Comsol software

TGC (H=0.314m)		2.10^4(s)	4.10^4(s)	6.10^4(s)	8.10^4(s)
Spectral code	C_{max}	0.6129	0.6130	0.6129	0.6129
	C_{min}	0.6047	0.6046	0.6047	0.6047
Comsol code	C_{max}	0.6133	0.6134	0.6132	0.6132
	C_{min}	0.6043	0.6042	0.6044	0.6044
TGC (H=0.628m)		5.10^4(s)	10^5(s)	2.10^5(s)	4.10^5(s)
Spectral code	C_{max}	0.6149	0.6157	0.6159	0.6159
	C_{min}	0.6027	0.6019	0.6017	0.6017
Comsol code	C_{max}	0.6149	0.6159	0.6164	0.6165
	C_{min}	0.6027	0.6017	0.6012	0.6011

Table 5 Variaton of C_{max} and C_{min}, in the spherical cavity, from the initial uniform state, C_0 to the stationary non uniform state for $R_i = 0.1$ m, $R_i = 0.2$ m, $e = R_o - R_i = 6.10^{-3}$ m obtained using the spectral method and Comsol software

Spherical cell (Ri=0.1m)		2.10^4(s)	4.10^4(s)	6.10^4(s)	8.10^4(s)
Spectral code	C_{max}	0.6162	0.6208	0.6224	0.6229
	C_{min}	0.6001	0.5969	0.5973	0.5972
Comsol code	C_{max}	0.6147	0.6184	0.6203	0.6213
	C_{min}	0.6025	0.5994	0.5985	0.5983
Spherical cell (Ri=0.2m)		5.10^4(s)	10^5(s)	2.10^5(s)	4.10^5(s)
Spectral code	C_{max}	0.6212	0.6279	0.6324	0.6345
	C_{min}	0.5949	0.5876	0.5855	0.5860
Comsol code	C_{max}	0.6148	0.6206	0.6272	0.6312
	C_{min}	0.6053	0.6019	0.5976	0.5935

reached after a time twice as long as that in the upper part (Fig. 8). On the other hand, the stationary state is reached simultaneously at the top and at the bottom of the TGC (Fig. 7).

A qualitative interpretation of this result is understandable. In the spherical configuration, all the streamlines ensuring the species separation converge at the same places (the upper and lower parts of the spherical configuration around $\theta = \pi$ and $\theta = 0$ and for all vertical planes $\phi = cst$.

In the TGC column, the contributions of the streamlines occur in distinct places ($z = 0$ and $z = H$ for all vertical planes $y = cst$). Even if the flow is

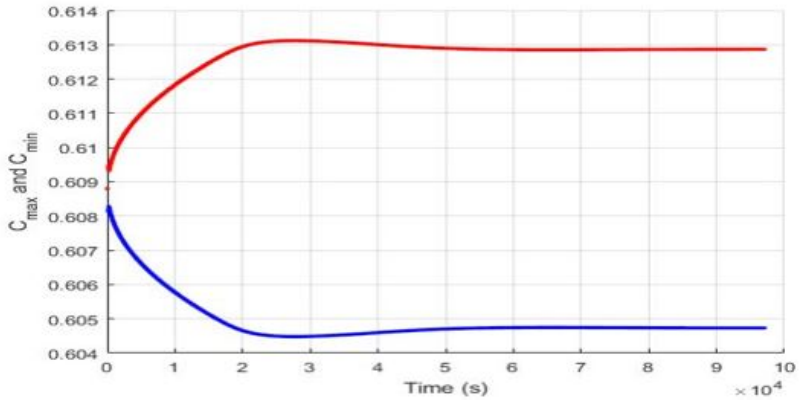

Fig. 7 Variation of C_{max} (in red) and C_{min} (in blue) as a function of time, in TGC, from the initial uniform state, C_0 to the stationary non uniform state for $H = \pi R_i$, $R_i = 0.1$ m and $e = 6.10^{-3}$ m, obtained using the spectral method

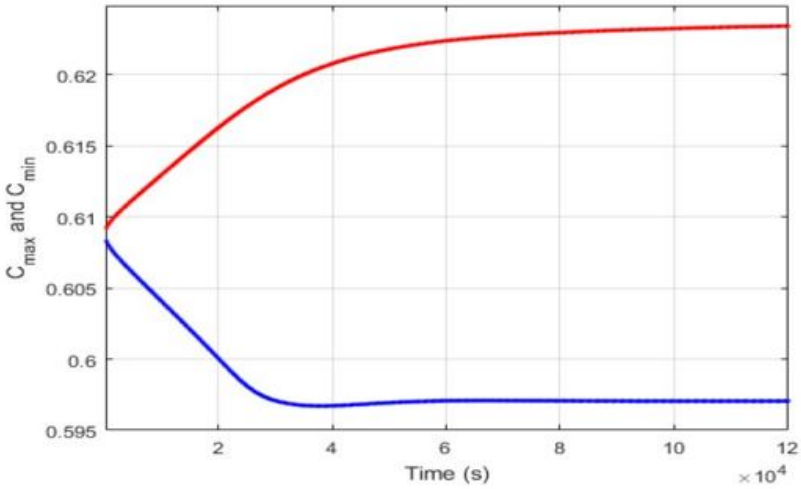

Fig. 8 Variation of C_{max} (in red) and C_{min} (in blue) as a function of time, spherical cavity, from the initial uniform state, C_0 to the stationary non uniform state for $R_i = 0.1$ m and $e = 6.10^{-3}$ m, obtained using the spectral method

axisymmetric in the spherical cavity and invariant by translation in the parallelepipedic cavity, these two properties of each of the convective flows have no effect on the time required to reach the stationary state. What is important is the time necessary for a fluid particle to move along its current line. The current lines in each of these two configurations have almost the same length and the velocity magnitude are very close leading to a separation time of the same order of magnitude.

6 Comparison of the importance of the species separation in the two configurations studied

At the steady state, the mass fraction of the denser constituent is higher in the bottom part than at the top part of each configuration studied. The volume of the binary solution of mass fraction $C > 0.66$ in each of these two configurations (conferred on Fig. 9 and Fig. 10) is calculated numerically and leads to:

$$V_{spherical} = \frac{2}{3}\pi[R_o^3 - R_i^3](1 - \cos\theta_1) = 7.356\ 10^{-4} m^3$$

and for the TGC to:

$$V_{TGC} = 2R_o eY_1 = 4.894\ 10^{-4} m^3$$

The amount of species separated at the bottom or top of the cells is about one and a half times larger for the spherical configuration than for the TGC.

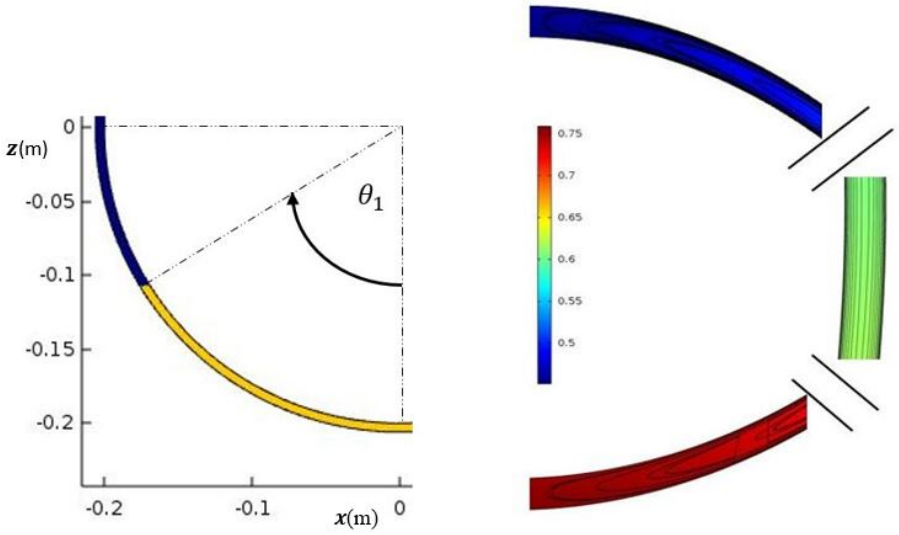

Fig. 9 (a) (on left) the amount of separation in a spherical cell, (b) (on right) Iso-C, streamlines in a spherical cell, $R_i = 0.2$ m, $e = 6.10^{-3}$ m, $\delta T = 10$ K and $K = 2.5\ 10^{-11}$ m^2

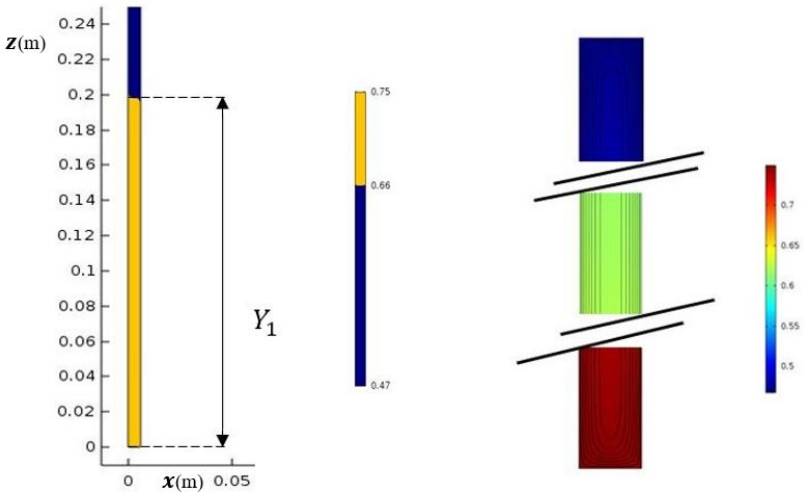

Fig. 10 (a) (on left) the amount of separation in a TGC, (b) (on right) Iso-C, streamlines in a a TGC, $H = 0.628$ m, $e = 6.10^{-3}$ m, $\delta T = 10$ K and $K = 2.5\ 10^{-11}$ m^2

7 Conclusion

Up to now, species separation was mainly obtained in vertical thermogravitational columns (TGC). At our knowledge, for flows between two spheres, in porous or fluid media, the works focused only on natural convection. In this study, numerical 2D and 3D simulations, were carried out in TGC and spherical configurations, for 4 values of R_i and 4 heights H and a moderate temperature difference between the walls. They showed that the flows remained 2D axisymmetric for the spherical configuration and invariant by translation in the horizontal direction, y, for the parallelepipedic vertical column. This result is due to the fact that in porous media the hydrodynamic boundary conditions are of the slip type on the walls.

Moreover, the analytical and numerical studies carried out in each of these two configurations showed that the differences in mass fractions between the top part and the bottom part of the spherical cavity are slightly higher than those obtained between the two ends of the TGC for the same thickness, $e = R_o - R_i$ and for a height $H = \pi R_i$.

At our knowledge, this is the first time that an analytical solution has been obtained in the spherical configuration.

In addition, we showed that the amount of species separated at the bottom or top of the cells is about one and a half times larger for the spherical configuration than for TGC column having similar geometric dimensions in two spatial directions.

Declarations

- Funding: NO FUNDING

- Conflict of interest/Competing interests (check journal-specific guidelines for which heading to use): NO CONFLICT OF INTEREST
- Ethics approval : YES
- Consent to participate: YES
- Consent for publication : YES
- Availability of data and materials : YES
- Code availability : YES
- Authors' contributions: ALL AUTHORS CONTRIBUTED EQUALLY TO THIS WORK

References

[1] R.C. Jones, W.H. Furry, The separation of isotopes by thermal diffusion, Rev. Mod. Phys. **18(2)**, 151-224 (1946).

[2] M. Lorenz, A. H. Emery, The packed thermal diffusion column, Chem. Eng. Sci. **11**, 16-23 (1959).

[3] A.H. Emery and M. Lorenz, Thermal diffusion in a packed column, AIChE Journal. **9(5)**, 660-663 (1963).

[4] Ph. Jamet, D. Fargue, P. Costesèque, Determination of the effective transport coefficients for the separation of binary mixtures of organic compounds into packed thermal diffusion columns, Chemical Engineering Science. **51(19)**, 4463-4475 (1996).

[5] D.E. Melnikov, V.M. Shevtsova, Separation of a binary liquid mixture in compound system: Fluid–porous–fluid, Acta Astronautica. **69**, 381–386 (2011).

[6] W. Köhler, K.I. Morozov, The Soret effect in liquid mixtures, J. Non-Equilibrium Thermodyn. **41(3)**, 151–197 (2016)

[7] J.K. Platten, M.M. Bou-Ali, J.F. Dutrieux, Enhanced molecular separation in inclined thermogravitational columns, J. Phys. Chem. **107 (42)**,11763–11767 (2003).

[8] M-C. Charrier-Mojtabi, B. Elhajjar, A. Mojtabi, Analytical and numerical stability analysis of Soret-driven convection in a horizontal porous layer, Phys. Fluids. **19**, 124104 (2007).

[9] B. Elhajjar, A.Mojtabi, M-C. Charrier-Mojtabi, Separation of a binary fluid mixture in a porous horizontal cavity, Physical Rev. **77(2)**, A.N. 026310 (2008).

[10] B. Elhajjar, A. Mojtabi, P. Costesèque, M-C. Charrier-Mojtabi, Separation in an inclined porous thermogravitational cell, Int. J. of Heat and Mass

transfer. **53(21-22)**, 4844-4851 (2010).

[11] A. Khouzam, A. Mojtabi, M-C. Charrier-Mojtabi, B. Ouattara, Species separation of a binary mixture in the presence of mixed convection, Int. J. Therm. Sci. **73**, 18–27 (2013).

[12] L. Yacine, A. Mojtabi, R. Bennacer, A. Khouzam, Soret-driven convection and separation of binary mixtures in a horizontal porous cavity submitted to cross heat fluxes, Int. J. Therm. Sci. **104**, 29–38 (2016).

[13] V. Yasnou, A. Mialdun, D. Melnikov, V. Shevtsova Role of a layer of porous medium in the thermodiffusion dynamics of a liquid mixture, Int. J. Heat and Mass Transfer, **143**, 118480 (2019).

[14] A. Mojtabi, B. Ouattara, D.A.S. Rees, M-C. Charrier-Mojtabi, The effect of conducting bounding horizontal plates on species separation in porous cavity saturated by a binary mixture, Int. J. of Heat and Mass transfer. **126**, 479-488 (2018).

[15] A. Mojtabi, A. Khouzam, Y. Loujaine, M-C. Charrier-Mojtabi, Analytical and numerical study of Soret mixed convection in two sided lid-driven horizontal cavity: Optimal species separation, Int. J. of Heat and Mass transfer. **139**, 1037-1046 (2019).

[16] B. Seta, E. Lapeira, D. Dubert, F. Gavalda, M.M. Bou-Ali, X. Ruiz, Separation under thermogravitational effects in binary mixtures, Eur. Phys. J. E. **42**, 58 (2019).

[17] M. Ouriemi, P. Vasseur, A. Bahloul, L. Robillard, Natural convection in a horizontal layer of binary mixture, Int. J. Therm. Sci. **45(8)**, 752-759 (2006).

[18] P. Costesèque, T. Pollak, J.K. Platten and M. Marcoux, Transient-state method for coupled evaluation of Soret and Fick coefficients, and related tortuosity factors, using free and porous packed thermodiffusion cells: Application to CuSO4 aqueous solution (0.25 M), Eur. Phys. J. E. **15**, 249-253 (2004).

[19] R. Peyret, Spectral Methods for Incompressible Viscous Flow, App. Math. Sciences, New York, (2002).